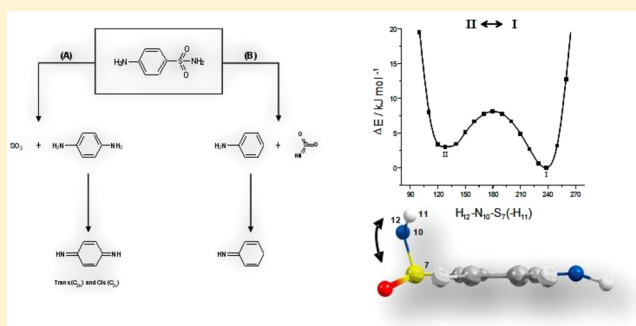


Conformational Landscape, Photochemistry, and Infrared Spectra of Sulfanilamide

Ana Borba,[†] Andrea Gómez-Zavaglia,^{†,‡} and Rui Fausto^{*,†}[†]Department of Chemistry, University of Coimbra, P-3004-535, Portugal[‡]Centro de Investigación y Desarrollo en Criotecología de Alimentos, Conicet La Plata, UNLP, RA-1900, Argentina

Supporting Information

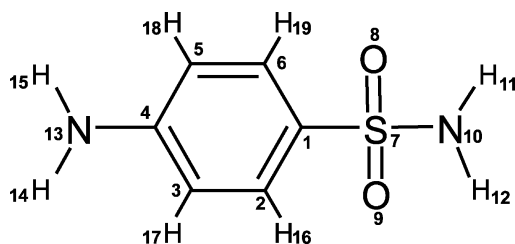
ABSTRACT: A combined matrix isolation FTIR and theoretical DFT(B3LYP)/6-311++G(3df,3pd) study of sulfanilamide (SA) was performed. The full conformational search on the potential energy surface of the compound allowed the identification of four different minima, all of them bearing the sulfamide nitrogen atom placed in the perpendicular orientation relatively to the aromatic ring and differing from each other in the orientation of the hydrogen atoms connected to the two nitrogen atoms of the molecule. All conformers were predicted to be significantly populated in the gas phase (at 100 °C, their relative populations were estimated as being 1:0.9:0.3:0.2). However, in agreement with the theoretically calculated low-energy barriers for conformational isomerization, in the low-temperature matrices, only the most stable conformer could be observed, with the remaining forms being converted into this form during matrix deposition (conformational cooling). The unimolecular photochemistry of matrix-isolated SA (in both argon and xenon) was also investigated. Upon broadband UV irradiation ($\lambda > 215$ nm), two photofragmentation pathways were observed: the prevalent pathway (A), leading to extrusion of sulfur dioxide and simultaneous formation of benzene-1,4-diamine, which then converts to 2,5-cyclohexadiene-1,4-diimine, and the minor pathway (B), conducting an γ -cleavage plus [1,3] H-atom migration from the sulfamide group to the aromatic ring, which leads to formation of iminosulfane dioxide and aniline, the latter undergoing subsequent phototransformation into cyclohexa-2,5-dien-1-imine. Finally, the crystalline polymorph of SA resulting from warming (265 K) the amorphous solid obtained from fast cooling of the vapor of the compound onto the cold (13 K) substrate of the cryostat was identified spectroscopically, and found to be the γ -crystalline phase, the one exhibiting in average longer H-bonds and an infrared spectrum resembling more that of the low temperature SA glass. Full assignment of the infrared spectra of this crystalline variety as well as of those of the β -polymorph room temperature crystalline sample and low temperature amorphous state was undertaken with help of theoretical results obtained for the crystallographically relevant dimer of SA.



INTRODUCTION

Sulfanilamide (or 4-aminobenzenesulfonamide; SA; Scheme 1) was synthesized for the first time more than one century ago.¹

Scheme 1. Schematic Representation of the Molecule of SA with Adopted Atom Numbering



It is the simplest representative of a large series of sulfonamides widely used in pharmaceutical chemistry and medicine. Its strong antibacterial activity and low toxicity for humans were discovered by Domagk in 1934 (Nobel Prize, 1939).²⁻⁴

Sulfanilamides were the first effective chemotherapeutic agents to be employed in the prevention and cure of bacterial infections in humans.²⁻⁷ Many other sulfonamides are also well-known antibacterial,⁸ anticancerous,⁹ carbonic anhydrase inhibitors,¹⁰ and anti-inflammatory agents.¹¹

The pharmacological relevance of SA has encouraged the study of its physicochemical properties, including polymorphism, an important issue in determining bioavailability.¹² Sulfanilamide was found to crystallize in at least four different polymorphs: α , β , γ , and δ (see Figure S1, Supporting Information).¹³⁻²¹ The occurrence of polymorphism in SA has been ascribed to the relevance of several types of intermolecular interactions in determining the crystal structures of the compound, in particular intermolecular hydrogen bonds of the N-H...O=S type and dispersion interactions between aromatic rings. These interactions

Received: October 9, 2012

Revised: January 7, 2013

Published: January 7, 2013

allow for establishment of different types of cross-linked three-dimensional networks, in a similar way as found, for example, for pyrazinamide.²²

The crystal structures of the α , β , and γ polymorphic forms were determined first in 1965.^{15,17,18} The thermodynamic studies of the compound carried out by Toscani and co-workers in the late nineties of the XX Century^{20,21} considered only these three polymorphs. The authors concluded that the α form was metastable in all conditions investigated, while both β and γ forms owned stability domains. The β form was found to be stable at room temperature, while the γ form corresponds to the most stable polymorph at high-temperature and high-pressure conditions, being a higher-energy enantiotropic form at normal pressure, where form β is the most stable polymorph.^{20,21} The structure of the δ polymorphic variety was obtained only recently,¹⁹ though it was known to exist for more than 30 years.^{23,24} In α , β , and γ polymorphs, both SA sulfonyl oxygen atoms are engaged in N–H...O=S interactions defining the primary H-bond network, while in polymorph δ only one sulfonyl oxygen atom per molecule participates in this hydrogen-bond network, forming two H-bonds with the sulfamide groups of two different neighbor molecules (see Figure S1).

The infrared (IR) spectra of several sulfonamides in the solid state and in solution were reported long time ago.²⁵ In the case of SA, both IR and Raman spectroscopic investigations, complemented by theoretical studies of the compound performed at the Hartree–Fock level of approximation, have been reported.^{26–30} More recently, López-Sánchez and co-workers³¹ have also studied the Raman spectrum of SA using a procedure based on a univariate calibration model that also allowed a rapid quantitative analysis of the compound, whereas Halim et al.²⁹ employed the polarizable continuum model (PCM) to investigate solvent effects on the geometry, vibrational spectra, solvation free energies, and dipole moment of SA.

The preferred conformations assumed by the molecule of sulfanilamide have also been investigated theoretically at different levels of theory, including semiempirical (PM3) and DFT-based methods.^{33–36} To the best of our knowledge, the study by Popova et al.³⁵ was the first work dealing specifically with the subject of conformational isomerism in SA. Two conformers of the molecule were predicted to exist, separated by 4.13 kJ mol⁻¹.³⁵ On the other hand, in a more recent work, Ildiz and Akyuz³⁶ concluded that the molecule has four conformers, differing in the relative orientation of the two amino groups.

The photochemistry of SA in solution was also addressed before.^{37,38} The general mechanisms of photofragmentation of sulfonamides and sulfonylureas have been investigated by Weiss et al.³⁹ Different types of photocleavages can take place upon photolysis of these molecules (Scheme 2), leading to the initial formation of various radicalic species. The radicals NH₂PhSO₂, NH₂SO₂, and NH₂SO₂Ph (ph = phenyl) were found to eliminate

SO₂ to give simple alkyl or aryl radicals, which then stabilize by recombination or by abstraction of hydrogen from the solvent.³⁹ In the specific case of SA, the radicals resulting from the different photolytic cleavages could be successfully trapped during the photolysis of the compound in aqueous solution.^{37,38} Recent studies on the photofragmentation of sulfa drugs in aqueous solutions⁴⁰ confirmed the previous results.^{38,39} Electron irradiation of SA in solution yielded four different products, one of them identified as corresponding to aniline.³⁸

With the general aim of contributing to the better understanding of the structural and spectroscopic properties of the compound and of its chemical reactivity, in the present study, we intend to achieve the following main objectives: (i) to obtain a more detailed structural and vibrational characterization of SA using a higher level of theory than those used in the previous studies. Specifically, it has been shown^{41,42} that the theoretical description of molecules containing the SO₂ fragment requires the use of highly polarized basis functions, so that a detailed investigation of the potential energy surface of SA was carried out in this study using the 6-311++G(3df,3pd) basis set. These calculations also provided fundamental data about the barriers for conformational isomerization, which proved to be of critical importance for the interpretation of the experimental results, in particular for the rationalization of the sole presence in these experimental conditions of the most stable conformer in the studied cryogenic matrices; (ii) to register and interpret the IR spectra of monomeric SA isolated in noble gas (Ar, Xe) cryogenic matrices and investigate its unimolecular photochemistry under these experimental conditions; (iii) to investigate the nature of the neat solid phases produced by fast deposition of the vapor of the compound onto a cooled (~10 K) substrate and after annealing of the initially formed solid phase to higher temperatures (within the 10–290 K temperature range).

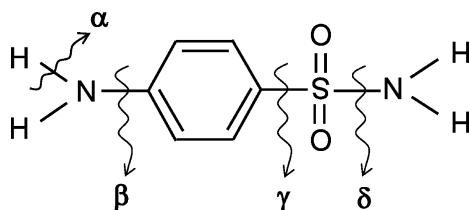
EXPERIMENTAL AND COMPUTATIONAL METHODS

Infrared Spectroscopy. Sulfanilamide and aniline were obtained from Aldrich and Acros Organic, respectively, purity 99%. The low temperature matrices were prepared by codeposition of the matrix gas (argon N60 or xenon N45, both obtained from Air Liquide) and SA or aniline sublimate, in an approximately 1000:1 concentration ratio, onto the cooled CsI substrate of the cryostat (APD Cryogenics close-cycle helium refrigeration system with a DE-202A expander). SA was placed in a mini-oven assembled inside the cryostat, the temperature of the mini-oven used to evaporate SA being, in all experiments, about 100 °C. The solid film of the neat compound was prepared in a way similar to that used to obtain the matrices, but in this case only vapors of the compound were deposited onto the CsI substrate of the cryostat.

Aniline was deposited from a specially designed effusive cell connected to the cryostat through a NUPRO SS-4BMRG needle valve with shut-off possibility. The valve nozzle and the sample compartment were thermostatted separately: the nozzle of the valve was kept at room temperature, and the sample compartment was cooled to 0 °C by immersing the ampule in an ice bath in order to reduce the vapor pressure of aniline and ensure a better control of the gaseous flux, guaranteeing an appropriate dilution of the matrices that avoids aggregation of SA. Accordingly, the obtained spectra reveal no features of aggregates, testifying that the compound is well isolated.

In the annealing experiments, the temperature was controlled and measured by a diode sensor connected to a Scientific Instruments digital temperature controller (model 9659) to within

Scheme 2. Schematic Representation of Previously Observed^{37–40} Photofragmentations of Sulfonamides (as Exemplified for SA)



$\pm 1^\circ$. The temperature variation during the annealing was done in steps of 2° in the matrix isolation experiments, and in steps of $10\text{--}20^\circ$, in the studies of the neat solid compound.

The IR spectra were collected with 0.5 cm^{-1} spectral resolution, on a Nicolet 6700 Fourier Transform infrared spectrometer equipped with a deuterated triglycine sulfate (DTGS) detector and a Ge/KBr beamsplitter.

In situ UV ($\lambda > 215\text{ nm}$) irradiation of the matrices was carried out through the outer quartz window of the cryostat, using a 500 W Hg(Xe) lamp (Newport, Oriol Instruments) set to provide 250 W at the sample position.

Computational Methodology. The quantum chemical calculations were performed with the Gaussian 03 suite of programs,⁴³ at the DFT(B3LYP) level of approximation,^{44–46} using the 6-311++G(d,p) and 6-311++G(3df,3pd) basis sets.^{47–50} Structures were optimized using the geometry direct inversion of the iterative subspace (GDIIIS) method,⁵¹ with the nature of the obtained stationary points being checked by inspection of the corresponding Hessian matrix. The B3LYP/6-311++G(3df,3pd) calculated vibrational frequencies were uniformly scaled by 0.978.⁵² Normal coordinate analyses were undertaken in the internal coordinate space, as described by Schachtschneider and Mortimer,⁵³ using a locally modified version of the program BALGA and the optimized geometries and harmonic force constants resulting from the B3LYP/6-311++G(3df,3pd) calculations. Potential energy profiles for internal rotation were calculated by performing a relaxed scan on the B3LYP/6-311++G(d,p) potential energy surface along the relevant coordinates, and the transition state structures for conformational interconversions were obtained using the synchronous transit-guided quasi-Newton (STQN) method.⁵⁴

RESULTS AND DISCUSSION

Conformational Landscape of the SA Monomer.

Sulfanilamide has five different internal degrees of freedom that can give rise to different conformers, the internal rotations around the $\text{N}_{10}\text{--S}_7$, $\text{N}_{13}\text{--C}_4$, and $\text{S}_7\text{--C}_1$ bonds and the inversions at the two nitrogen atoms (N_{10} , N_{13}). After a systematic conformational search on the B3LYP/6-311++G(d,p) potential energy surface of the molecule, four different minima were located (Figure 1), which were subsequently reoptimized at the B3LYP/6-311++G(3pd,3df) level of approximation. Table 1 displays the

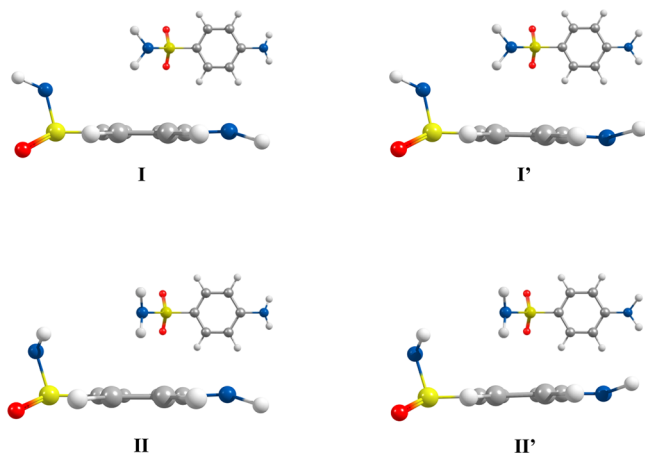


Figure 1. DFT(B3LYP)/6-311++G(3pd,3df) optimized structures of the conformers of SA. Two perspectives are provided, one with the viewpoint placed above the ring (top) and the other with the viewpoint along the major axis of the molecule.

Table 1. Zero-Point Corrected Relative Energies (ΔE), Gibbs Energies (ΔG), and Dipole Moments ($|\mu|$) for SA Conformers^a

conformer ^b	B3LYP/6-311++G(3df,3pd)			B3LYP/6-311++G(d,p)		
	ΔE^c	ΔG	$ \mu $	ΔE^d	ΔG	$ \mu $
I	0.00	0.00	4.9	0.00	0.00	5.1
I'	0.26	0.45	5.8	0.20	0.19	6.0
II	1.35	4.36	7.1	3.36	7.21	7.6
II'	1.78	4.69	7.8	3.83	7.58	8.3

^aEnergies in kJ mol^{-1} ; dipole moments in Debye. ^bConformers are depicted in Figure 1. ^cAbsolute energy for conformer I is $-2341041.05\text{ kJ mol}^{-1}$. ^dAbsolute energy for conformer I is $-2340801.72\text{ kJ mol}^{-1}$.

calculated relative energies, Gibbs free energies and dipole moments of the obtained minima. The corresponding optimized geometrical parameters are provided in Table S1 (Supporting Information).

In all SA minima, the sulfamide nitrogen atom (N_{10}) is placed in a perpendicular orientation relatively to the aromatic ring. The hydrogen atoms connected to this nitrogen atom can be either directed toward the ring (forms II and II'; Figure 1) or pointing to the opposite direction (I, I'). In turn, the hydrogen atoms belonging to the slightly nonplanar aniline group can be located in the same side of the ring as the sulfamide NH_2 group or in the opposite side. Conformers differing only in the orientation of the aniline group (pairs of conformers I/I' and II/II') can be converted to each other by rotation about the $\text{N}_{13}\text{--C}_4$ or $\text{S}_7\text{--C}_1$ bonds as well as inversion at the N_{13} atom. As shown in Figure S2A–D, rotation about the $\text{N}_{13}\text{--C}_4$ bond requires activation energies larger than 30 kJ mol^{-1} , and that around the $\text{S}_7\text{--C}_1$ bond needs to overcome barriers of about 10 or 15 kJ mol^{-1} , depending on the orientation of the sulfamide NH_2 group: in the case of the I/I' conversion, the transition states contain a stabilizing interaction of the $\text{C--H}\cdots\text{NH}_2$ type, which reduces the associated energy barrier; for the conversion II/II', this stabilizing interaction is replaced by $\text{C--H}\cdots\text{H}_2\text{N}$ repulsive interactions, leading to higher energy barriers. On the other hand, the energy barriers associated with the inversion at N_{13} are only about 1.5 kJ mol^{-1} (lower than 1 kJ mol^{-1} , if zero-point corrections were taken into account), Figure 2A,B. In practical terms, this last result allows us to conclude that in the matrix isolation experiments the higher energy conformer in each pair of structures differing in the orientation of the aniline NH_2 group (I' and II') will quickly relax to the corresponding most stable form (I or II) during deposition of the matrix (conformational cooling^{54,55}).

In agreement with previous investigations,^{32,33} conformer I is predicted to be the most stable form at both levels of theory used in the present study. This conformer is stabilized by the presence of favorable interactions between the antiparallel bond-dipoles associated with the N--H and S=O sulfamide bonds. On the other hand, conformer II is stabilized by H-bond type interactions of $\text{NH}\cdots\pi$ nature, but destabilized by the repulsion between the lone electron pairs of the oxygen atoms and N_{10} . On the whole, conformer I results the most stable one.

Figures S2E and 2C depict the B3LYP/6-311++G(d,p) relaxed potential energy profiles corresponding to the possible interconversion pathways between conformers I and II: rotation about the $\text{N}_{10}\text{--S}_7$ bond and inversion at N_{10} . The calculated barrier for the rotation about the $\text{N}_{10}\text{--S}_7$ bond was found to be $\sim 14\text{ kJ mol}^{-1}$ in the $\text{II} \rightarrow \text{I}$ direction (Figure S2E); that associated with the inversion at N_{10} amounts to about 6 kJ mol^{-1} (Figure 2C). The last barrier is low enough to be overcome during matrix

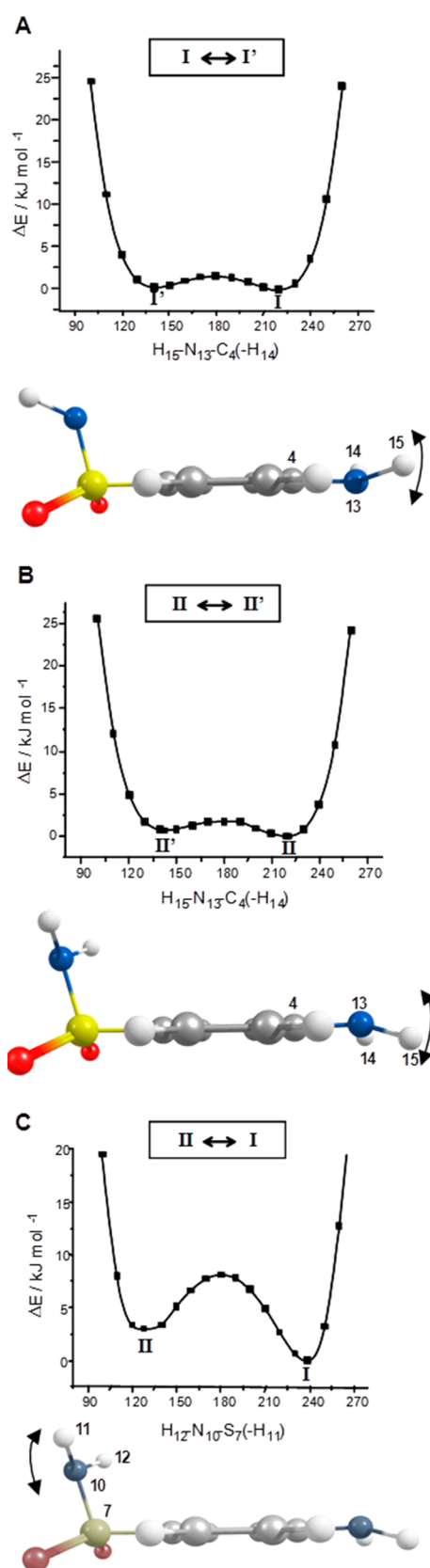


Figure 2. DFT(B3LYP)/6-311++G(d,p) calculated potential energy profiles corresponding to the inversion at the N_{13} and N_{10} atoms, resulting in (A, B) interconversion between the pairs of conformers of SA, which differ by the relative orientation of the aniline NH_2 group (I, I' and II, II'), and (C) interconversion between I and II. The zero in the energy scales corresponds always to the energy of the most stable conformer I.

deposition,^{54,55} so that the higher energy conformer II can also be expected to convert into the most stable conformer I.

In conclusion, in the gas phase equilibrium SA is predicted to exist in four different conformers, all with significant populations. Taking into account the calculated relative Gibbs energies for each conformer (Table 1), the expected relative populations for the four conformers in the gas phase at $\sim 100^\circ C$ (the temperature used to sublime the compound in the matrix isolation experiments) are $p_I/p_{I'}/p_{II}/p_{II'} = 1:0.9:0.3:0.2$. However, in view of the low conformational isomerization barriers, conformational conversion can be expected to easily take place during deposition of the cryogenic matrices, resulting in the likely sole observation of the most stable conformer I in the as-deposited matrices. Note that, in the case of the pair I/I', the predicted energy difference is only 0.26 kJ mol^{-1} (see Table 1), which would in principle let still opened the perspectives of observing the higher energy form as minor species in the matrices at 15 K, because, according to the Boltzmann distribution, about 10% of this conformer should exist at 15 K. However, as it will be shown in detail in the next section, experimental evidence of the presence of conformer I' in the matrices could not be obtained. This seems to indicate that the calculated energy difference between the two conformers is slightly underestimated (a value like 0.35 kJ mol^{-1} , on the other hand, would lead to an expected population of less than 5% for I', i.e., below the limit of experimental detection).

IR Spectra of Matrix-Isolated SA. All sulfanilamide conformers belong to the C_s symmetry point group and have 51 fundamental vibrations, all being infrared active. Table S2 (Supporting Information) displays the definition of the symmetry coordinates of SA used in the normal coordinates analysis undertaken in this study. The B3LYP/6-311++G(3df,3pd) calculated vibrational wavenumbers and infrared intensities for the four SA conformers, as well as the characterization of the normal coordinates in terms of potential energy distribution (PED), are given in Tables S3–S6 (Supporting Information).

Figure 3 depicts the IR spectra of SA in argon and xenon matrices, obtained immediately after deposition at 15 and 30 K, respectively, together with the calculated spectrum for conformer I (calculated spectra for the four SA conformers can be found in Figure S3, Supporting Information). The proposed band assignments are shown in Table 2. Considering the excellent agreement between the theoretical and experimental spectra (in particular above 1000 cm^{-1} ; see Figure 3), the general assignment of the experimental bands was straightforward. The experimental spectrum obtained in argon matrix is dominated by three intense bands at 1621, 1382 (with shoulder at 1385), and 1170 cm^{-1} (1619, 1377, and $1167/1161 \text{ cm}^{-1}$, in xenon), which have theoretical counterparts at 1624, 1347, and 1140 cm^{-1} (scaled wavenumbers), respectively, and are assigned to the anilinic NH_2 scissoring mode and SO_2 stretching modes (asymmetric and symmetric; see Table 2). In the high frequency range, the four expected NH_2 stretching modes give rise to well-separated site-split bands both in argon and in xenon matrices. The two bands due to the anilinic NH_2 group in SA are observed at $3528/3522$ and $3433/3429 \text{ cm}^{-1}$, at close frequencies to those observed for the parent aniline isolated in the same matrix ($3503/3499/3497$, $3415/3412/3410 \text{ cm}^{-1}$). This is also true for most of the remaining bands due to this NH_2 group (e.g., the δNH_2 , γNH_2 , and ωNH_2 bands are observed at 1621, 1082, and 429 cm^{-1} in SA, and centered at 1619, 1090, and 420 cm^{-1} in aniline, respectively).

The most interesting issues to note in the experimental spectra of SA are (i) the increased relative intensity, compared to the

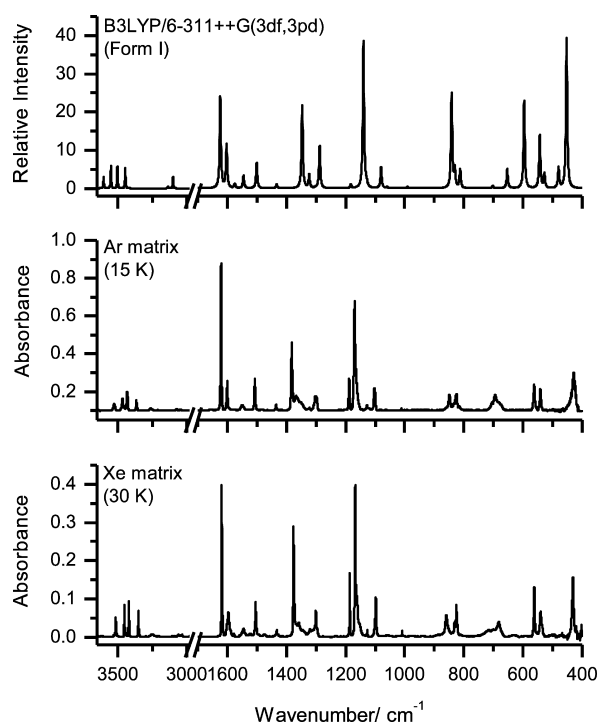


Figure 3. Experimental infrared spectra (3650–400 cm^{-1} spectral range) of SA in argon (15 K) and xenon (30 K) matrices, and B3LYP/6-311++G(3df,3pd) calculated spectra for conformer I. The calculated spectrum was simulated using Lorentzian functions with full-width-at-half-maximum of 5 cm^{-1} , wavenumbers being scaled by 0.978. Note that the peak intensities in the simulated spectra (arbitrary units of “relative intensity”) are several times less than the calculated intensities (in km mol^{-1} and shown in Table 2).

theoretical predictions, of the bands due to the symmetric stretching of the ring C–H bonds *ortho* to the anilinic NH_2 group [$\delta\text{C–H}$]²: 1188/1187 cm^{-1} in argon and 1186 cm^{-1} in xenon; see Figure 3 and Table 2], (ii) the extensive site-splitting (in particular, in the argon matrix spectrum) observed for the C–N and S–N stretching bands, and (iii) most importantly, the considerable blue shift of the observed bands due to the wagging vibration of the sulfamide NH_2 group (705/694 and 702 cm^{-1} , in argon and xenon matrix, respectively) compared to the calculated data (596 cm^{-1}). The last result comes in line with previously reported data⁵⁶ for other molecules bearing pyramidalized NH_2 groups in the gas phase, which in the solid cryogenic matrices assume configurations considerably more planar due to the solid state packing forces. The NH_2 wagging vibration is extremely sensitive to the degree of pyramidalization at the N atom. Note that, on the contrary, the wagging vibration of the anilinic NH_2 group in SA is predicted much better by the calculations (calcd.: 452 cm^{-1} ; exp.: 429, 431 cm^{-1} , in argon and xenon, respectively; see Table 2), indicating that the geometry of this group does not change significantly in the matrices relative to the free molecule in the gas phase.

In spite the great similarity between the spectra of all conformers (see Tables S3–S6), the sole presence in the matrices of conformer I was confirmed by the results of the performed annealing experiments. Once again, the potential energy landscape of SA revealed by the theoretical calculations appeared as the key information for the interpretation of the experimental results, allowing to conclude on the sole existence of conformer I in the matrix. Indeed, no spectral changes ascribable to any conformational conversion could be observed upon

annealing the argon matrix up to 45 K or even by annealing the xenon matrix up to 85 K. According to the Barnes relationship,⁵⁷ an isomerization process with a barrier of about 6 kJ mol^{-1} (II \rightarrow I) should start to be observed in a matrix at a temperature as low as about 25 K.

UV-Induced Photochemistry for the Matrix-Isolated SA. In situ irradiation (broadband, $\lambda > 215$ nm; 120 min) of the matrix-isolated SA monomer allowed the investigation of its photochemistry under these experimental conditions. Scheme 3 summarizes the results of the photochemical experiments, showing the reaction paths corresponding to the observed photoprocesses. Identification of the photoproducts was made by comparing the bands appearing upon irradiation of the matrices with the calculated spectra for possible reaction products and also taking into account available data for some of these species.^{58,59} Below, the discussion is centered on the results obtained in argon. Those obtained in xenon were found to be identical.

Identification of SO_2 and iminosulfane dioxide (SO_2NH) in the spectra of the irradiated matrices was made easily (see Figure 4). The spectrum of matrix-isolated SO_2 is well-known⁵⁸ (see also Table 3). The most intense bands of this molecule are due to the two νSO_2 stretching modes (symmetric and antisymmetric) and were observed in the SA irradiated argon matrix at 1372–1320 cm^{-1} (broad structured band with a prominent component at the higher frequency) and 1166 cm^{-1} . These frequency values are in good agreement with the literature data for matrix-isolated SO_2 (1355, 1152 cm^{-1}),⁵⁸ but clearly evidencing the fact that the photoproducted SO_2 is interacting in the matrix cage with another photoproduct simultaneously produced from SA in the present photolysis experiments. The SO_2 bending mode was observed at 515 cm^{-1} (Figure S4), also in good agreement with the literature data (520 cm^{-1}).⁵⁸ On the other hand, the IR spectrum of iminosulfane dioxide has never been reported before. Nevertheless, all bands of the B3LYP calculated IR spectrum for this compound with frequencies in the studied spectral range could be assigned to experimental bands appearing in the spectra of the UV-irradiated SA matrices. For this compound, the most intense bands correspond also to the two νSO_2 stretching modes, predicted to occur at 1371 and 1274 cm^{-1} . In the SA photolyzed argon matrix, the bands due to these vibrations were observed at 1387 and 1293 cm^{-1} , respectively (see Figure 4). The third most intense band of SO_2NH , as predicted by calculations, corresponds to the $\delta\text{N–H}$ mode, expected to occur around 1053 cm^{-1} . Accordingly, a band was observed at 1062 cm^{-1} in the spectrum of the SA photolyzed argon matrix, which was then assigned to this vibration (Figure 4 and Table 3). Other less intense bands, observed at 3436, \sim 1005, and 662 cm^{-1} in argon, were also ascribed to vibrations of SO_2NH , corresponding to the calculated modes predicted to occur at 3431 ($\nu\text{N–H}$), 964 ($\nu\text{S=N}$), and 656 ($\gamma\text{N–H}$) cm^{-1} .

The unequivocal observation of both SO_2 and SO_2NH suggested occurrence of two different pathways. This is also suggested by the obtained kinetic data and relative product amounts, as shown in Figure S5. The most probable pathway to production of SO_2 should be the one leading to the simultaneous formation of benzene-1,4-diamine (BDA; see Scheme 3). On the other hand, SO_2NH could be produced together with aniline. As shown in detail below, both BDA and aniline were, in fact, identified in the UV-photolyzed SA matrices. In addition, the comparison of the relative intensities of the bands ascribable to SO_2 and SO_2NH led to the conclusion that the formation of SO_2 corresponds to the preferred reaction pathway, while the second reaction channel, leading to the production of SO_2NH , is a minor

Table 2. Observed Wavenumbers for the Matrix Isolated SA Monomer with Band Assignments^a

approximate description	calculated frequency	intensity	observed argon (15 K)	observed xenon (30 K)
$\nu(\text{NH}_2)_{\text{as}} 2$	3602	24	3528/3522	3514/3511 (sh)
$\nu(\text{NH}_2)_{\text{as}} 1$	3550	46	3473/3464	3455/3452/3446 (sh)
$\nu(\text{NH}_2)_{\text{s}} 2$	3502	45	3433/3429	3420/3417 (sh)
$\nu(\text{NH}_2)_{\text{s}} 1$	3446	43	3372/3365	3354/3351
$\nu(\text{C-H})' 1$	3138	3	3075	3060
$\nu(\text{C-H})'' 1$	3138	1		
$\nu(\text{C-H})' 2$	3101	14	3046	3043/3034
$\nu(\text{C-H})'' 2$	3100	10		
$\delta(\text{NH}_2) 2$	1624	189	1621	1619
ν ring 5	1603	89	1600	1596
ν ring 4	1575	9	1582	1578
$\delta(\text{NH}_2) 1$	1545	26	1550	1545
$\delta(\text{C-H})'' 1$	1501	52	1508/1506 (sh)	1504/1502 (sh)
ν ring 3	1433	8	1435	1433
$\nu(\text{S=O})_{\text{as}}$	1347	171	1385 (sh)/1382	1377
ν ring 6	1323	28	1366/1363/1359	1360/1358
$\delta(\text{C-H})' 1$	1302	1	1322	1320
$\nu(\text{C-N})$	1288	87	1303/1301/1299/1297	1300/1296
$\delta(\text{C-H})'' 2$	1183	7	1188/1187	1186
$\nu(\text{S=O})_{\text{s}}$	1140	303	1170	1167/1161
$\delta(\text{C-H})' 2$	1129	8	1127	1127
ν ring 2	1080	43	1102	1098
$\gamma(\text{NH}_2) 1$	1060	3	1093	1092
$\gamma(\text{NH}_2) 2$	1048	1	1082	1077
δ ring 1	991	4	1012	1008
$\gamma(\text{C-H})'' 1$	965	0.1	n.o.	n.o.
$\gamma(\text{C-H})' 1$	949	0.04	n.o.	n.o.
$\nu(\text{S-N})$	842	195	882/862/833	888/870/831
$\gamma(\text{C-H})' 2$	831	37	849/847 (sh)	859
ν ring 1	813	38	827/825	826/824 (sh)
$\gamma(\text{C-H})'' 2$	811	0.3	816	812
τ ring 1	702	6	713	716
$\nu(\text{S-C})$	654	41	683/676	683
δ ring 3	636	0.2	637	635
$w(\text{NH}_2) 1$	596	179	705/694	702
$\delta(\text{N-SO}_2)_{\text{s}}$	544	110	562	561
$\gamma(\text{C-N})$	527	32	542	540
$\delta(\text{N-SO}_2)_{\text{as}'}$	479	38	465	467
$w(\text{NH}_2) 2$	452	314	429	431

^aCalculated frequencies (scaled by 0.978) in cm^{-1} , calculated intensities in km mol^{-1} . ν , bond stretching; δ , bending; γ , rocking; τ , torsion; w , wagging; s , symmetric; as , antisymmetric, n.o.; not observed; (sh), shoulder. See Table S2 for definition of coordinates.

one. When the calculated band intensities are used as reference in these estimations (see Figure S5), a branching ratio of $\sim 2:1$, favoring pathway A in Scheme 3, was obtained.

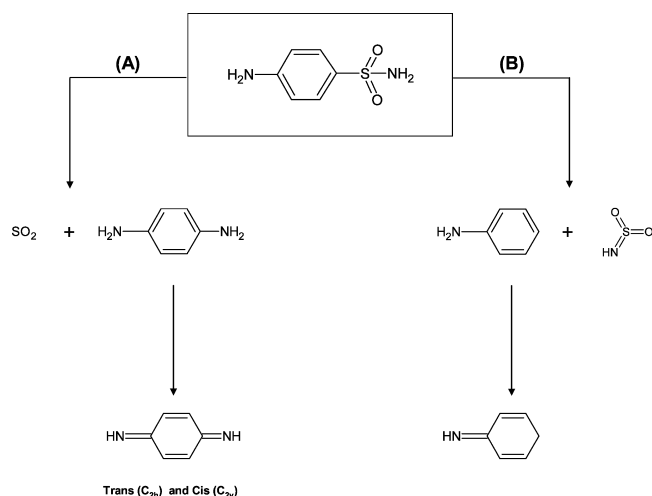
Photochemical Pathway A. In the major photochemical pathway A, BDA is formed together with SO_2 . BDA has been studied before, and its IR spectrum in argon matrix is known.⁵⁹ Moreover, the photochemistry of this compound in that medium was also investigated before,⁵⁹ and the phototransformation of SA into 2,5-cyclohexadiene-1,4-diimine (CHD) was observed, in a process involving formation of the benzene-1,4-diamine radical (4-aminoanilino radical).

The observed products of this pathway can result from a direct photolysis of SA, with simultaneous cleavage of the C-S and S-N bonds and extrusion of SO_2 , followed by recombination of the initially formed NH_2Ph and NH_2 radicals. Alternatively, they may be the final products of a more complex reaction involving the initial formation of the NH_2Ph and NH_2SO_2 radicals, with the subsequent release of SO_2 and further

recombination of the first formed NH_2Ph radical with the NH_2 radical formed in the secondary photolysis of NH_2SO_2 . Because neither NH_2SO_2 nor NH_2 could be experimentally observed, the precise mechanism for this pathway shall remain an open question.

Figure 5 shows selected spectral regions of the IR spectrum of the SA photolyzed ($\lambda > 215$ nm; 120 min) argon matrix, where the most intense characteristic bands of BDA, as well as of its expected photoproduct CHD, can be observed. The complete list of band assignments proposed for these two species is given in Table 3. A few bands were also tentatively ascribed to the 4-aminoanilino radical intermediate (see Table S7, Supporting Information). The values of the observed frequencies in the present study are in good agreement with both the theoretically obtained frequencies and the previously reported vibrational data for BDA, CHD (which as previously reported can be produced in two different isomeric forms, *cis* and *trans*; see Figure 5) and 4-aminoanilino radical (see Tables 3 and S7).

Scheme 3. Observed Reactions Resulting from In Situ Broadband UV ($\lambda > 215$ nm) Irradiation of SA Isolated in Rare Gas Matrices



From the relative intensities of the bands of the different species, one could conclude that the two CHD isomers were produced in nearly equal amounts, as it could be anticipated by taking into account the symmetry of the BDA precursor. On the other hand, at the end of the irradiation time (120 min.), the BDA/CHD population ratio was found to be $\sim 1:1$ (see Figure S5), that is, once produced from SA, BDA undergoes rather extensive photoconversion into CHD.

Photochemical Pathway B. The second (minor) SA photochemical pathway leads to formation of SO_2NH and aniline. In the present study, aniline was isolated in argon matrix and

subjected to the same irradiation conditions as SA. The most intense bands observed in the as-deposited spectrum of aniline in argon matrix closely match a series of bands appearing in the spectra of the photolyzed SA matrix (see Figure 6 and Table 3). The small observed differences in the band positions and band profiles in the two spectra are in agreement with the expected association of the aniline molecules formed from photolysis of SA with the SO_2NH molecules formed in the same matrix cage, in a similar way as observed for the pair SO_2/BDA (see above). The same applies to the bands ascribed to the identified aniline photoproduct (cyclohexa-2,5-dien-1-imine; CDI) in the spectra of the two photolyzed matrices (aniline and SA photolyzed matrices; see Figure 6). CDI is the photoproduct of aniline equivalent to the CHD photoproduct of BDA, resulting from cleavage of one of the N–H bonds. However, in the case of aniline, only one hydrogen atom is produced and, instead of reacting with a second hydrogen atom as occurs in the $\text{BDA} \rightarrow \text{CHD}$ reaction, it recombines with the aniliny radical through attack at the *para* position of this latter species. Note that no evidence was found of production of the species resulting from recombination of the H atom with the aniliny radical through attack at the *ortho* or *meta* positions. Very interestingly, this reaction resembles very much that observed in the case of matrix-isolated phenol and phenol- d_5 ,⁶⁰ where the photochemical cleavage of the O–H bond was found to occur upon UV irradiation, with the final product being 2,5-cyclohexadienone. Spectroscopic detection of phenoxyl radical could also be achieved in that study,⁶⁰ while no evidence was found of production of either 2,4-cyclohexadienone, the product resulting from recombination of the H atom with the phenoxyl radical through attack at the *ortho* position, or the bicyclo compound putatively produced through attack to the *meta* position. In the

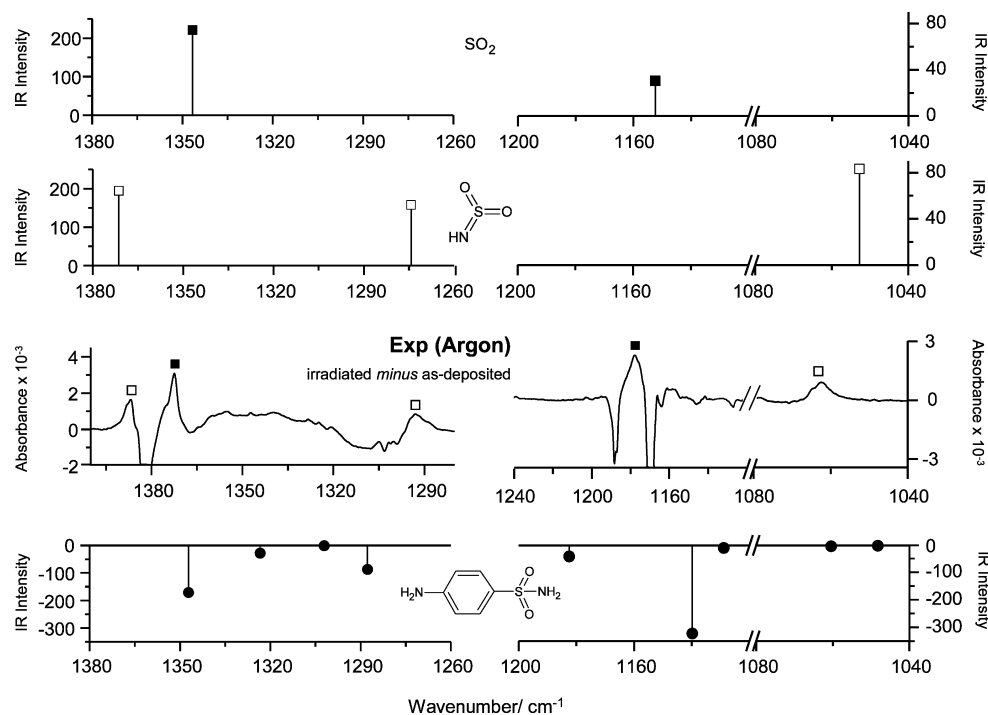


Figure 4. Results of UV ($\lambda > 215$ nm) irradiation of matrix isolated SA (argon matrix data; xenon matrix data are identical): selected spectral ranges showing the production of SO_2 and SO_2NH . Bottom to top: B3LYP/6-311++G(3pd,3df) calculated IR spectrum of SA (spectrum was multiplied by -1), experimental difference spectrum (irradiated matrix minus as-deposited matrix; bands pointing down belong to SA, while those pointing up belong to photoproducts), calculated spectrum of SO_2 , and calculated spectrum of SO_2NH . The shift of the wavenumber scale of the experimental spectrum relative to the calculated was done to allow a better comparison between the two sets of data.

Table 3. Experimental and Calculated [B3LYP/6-311++G(3df,3pd); Scaled by 0.978] Vibrational Frequencies (ν ; cm^{-1}) and Calculated IR Intensities (I , km mol^{-1}) for the Observed Photoproducts of SA Monomer Isolated in Argon and Xenon Matrices^a

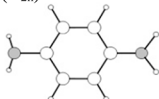
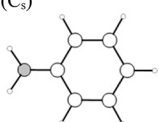
		Observed		Calculated		Literature (Ar matrix)	
		Argon	Xenon	ν I	ν I	ν	Ref.
SO₂ (C _{2v})							
$\nu(\text{SO}_2)_{\text{as}}$	B ₂	1372-1320	1367-1330	1346.7	220.9	1355	[58]
$\nu(\text{SO}_2)_{\text{s}}$	A ₁	1166	1165	1152.4	30.6	1152	[58]
$\delta(\text{SO}_2)$	A ₁	515	517	507.5	29.0	520	[58]
Benzene-1,4-diamine (BDA) (C _{2h})							
							
$\nu(\text{NH}_2)_{\text{as}}$	A _u	3469	3469	3559.5	23.5	3477	[59]
$\nu(\text{NH}_2)_{\text{s}}$	B _u	3437	3455	3470.7	18.4	3467	[59]
$\delta(\text{NH}_2)$	B _u	1619 sh ^b	1617 sh ^b	1618.1	105.1	1616	[59]
ν ring	B _u	1521	1528/ 1528	1516.0	215.7	1521	[59]
ν ring	A _u	1321 ^b	1320 ^b	1316.4	20.3	1322	[59]
$\delta(\text{C-H})$	A _u	1142 sh	1137	1132.1	15.3	1128	[59]
$\gamma(\text{NH}_2)$	A _u	1062 ^b	1060 ^b / 1057 ^b	1042.9	1.5	1032	[59]
$\gamma(\text{C-H})$	B _u	820	818	824.4	92.9	822	[59]
$\gamma(\text{C-H})$	B _u	765 / 762	762	755.4	3.0	763	[59]
2,5-cyclohexadiene-1,4-diimine (CHD)							
<i>trans</i> (C _{2h})				<i>cis</i> (C _{2v})			
							
$\nu(\text{N-H})_{\text{as}}$ (<i>trans</i>)	B _u	3367	3360	3365.0	11.9	n.o.	[59]
$\nu(\text{C=N})$ (<i>cis</i>)	B ₂	1593	1592/ 1591/	1616.3	140.2	1594	[59]
$\nu(\text{C=N})$ (<i>trans</i>)	B _u		1590	1617.1	138.0		[59]
ν ring (<i>cis</i>)	B ₂	1420	1416	1420.8	22.9	1426	[59]
$\delta(\text{C-H})$ (<i>trans</i>)	B _u	1360	1360	1360.9	20.4	1364	[59]
$\delta(\text{C-H})$ (<i>cis</i>)	B ₂	1321 ^b	1320 ^b / 1318	1316.4	60.0	1315	[59]
$\delta(\text{N-H})$ (<i>trans</i>)	B _u	1173/ 1166	1172	1169.2	68.9	1170/ 1165	[59]
$\delta(\text{C-H})$ (<i>cis</i>)	A ₁	1062	1060/ 1057	1046.5	16.2	1056	[59]
$\delta(\text{C-H})$ (<i>trans</i>)	B _u			1045.9	77.6		[59]
w(N-H) (<i>cis</i>)	B ₁	900	899	917.5	98.8	906	[59]
w(N-H) (<i>trans</i>)	A _u	876 ^b / 875 ^b	873 ^b	895.3	152.8	881	[59]
$\gamma(\text{C-H})$ (<i>cis</i>)	B ₁	860	858	869.9	39.6	856	[59]
SO₂NH (C _s)							
$\nu(\text{N-H})$	A'	3436	3422	3430.8	65.7		
$\nu(\text{SO}_2)_{\text{as}}$	A'	1387 ^b	1383 ^b / 1380 ^b	1371.4	194.4		
$\nu(\text{SO}_2)_{\text{s}}$	A'	1293	1291	1274.3	158.0		
$\delta(\text{N-H})$	A'	1062 ^b	1060 ^b / 1057 ^b	1052.7	83.3		
$\nu(\text{S=N})$	A'	1005/ 1003	1001	964.2	38.2		
$\gamma(\text{N-H})$	A''	662	663	656.0	71.0		
$\delta(\text{SO}_2)$	A'	515 ^b	517 ^b	507.7	20.5		
Aniline (C _s)							
							
$\delta(\text{NH}_2)$	A'	1619 sh ^b	1617 sh ^b	1621.9	131.4	1620/ 1624	
ν ring	A'	1608	1604	1605.9	32.9	1608	
$\delta(\text{C-H})$	A'	1500	1497	1496.9	59.0	1503	
$\nu(\text{C-N})$	A'	1297	1295	1264.9	72.2	1280/ 1282/ 1283	
$\gamma(\text{C-H})$	A'	876 ^b / 875 ^b	873 ^b	872.7	7.2	877/ 875	
$\gamma(\text{C-H})$	A'	755/ 749	762	745.9	73.6	757/ 756/ 755	
w(NH ₂)	A'	555	545	564.4	203.5	690/ 688	

Table 3. continued

		Observed		Calculated		Literature (Ar matrix)	
		Argon	Xenon	v I	v	v	Ref.
<i>Cyclohexa-2,5-dien-1-imine (CDI)</i> (C _s)							
v(C=C)s	A'	1650	1647	1680.4	59.5	1649	
v(C=N)	A'	1608	1611	1600.3	78.8	1608	
δ(N-H)	A'	<i>1387^b</i>	<i>1383^b / 1380^b</i>	1414.7	28.2	1386	
δ(CH ₂)	A'			1409.5	18.4		
w(CH ₂)	A'	1351/ 1348	1350/ 1341	1354.8	7.5	1344	
δ(C-H)	A'	1325	1331/ 1330	1328.5	19.5	1329	
δ(C-H)	A'	1166	1165	1165.5	24.6	1166/ 1165	
δ ring	A'	<i>1062^b</i>	<i>1060^b / 1057^b</i>	1094.7	31.5	1108/ 1107	
w(N-H)	A''	946	953/ 945	933.4	25.0	938/ 925/ 923	
γ ring	A''	888/ 887	885	892.3	49.1	885/ 884	
γ(C-H)	A'	<i>876^b / 875^b</i>	<i>873^b</i>	865.0	12.6	871	
γ ring	A''	819	818	820.3	17.8	814	

^aOnly the observed bands are shown: ν , stretching; δ , bending; γ , rocking; w, wagging; sh, shoulder; s, symmetric; as, asymmetric. Experimental data for aniline and CDI obtained in this work (aniline was deposited in argon matrix at 10 K and irradiated ($\lambda > 215$ nm) in situ). ^bBand assigned to more than one species; *italic style* indicates minor contributors.

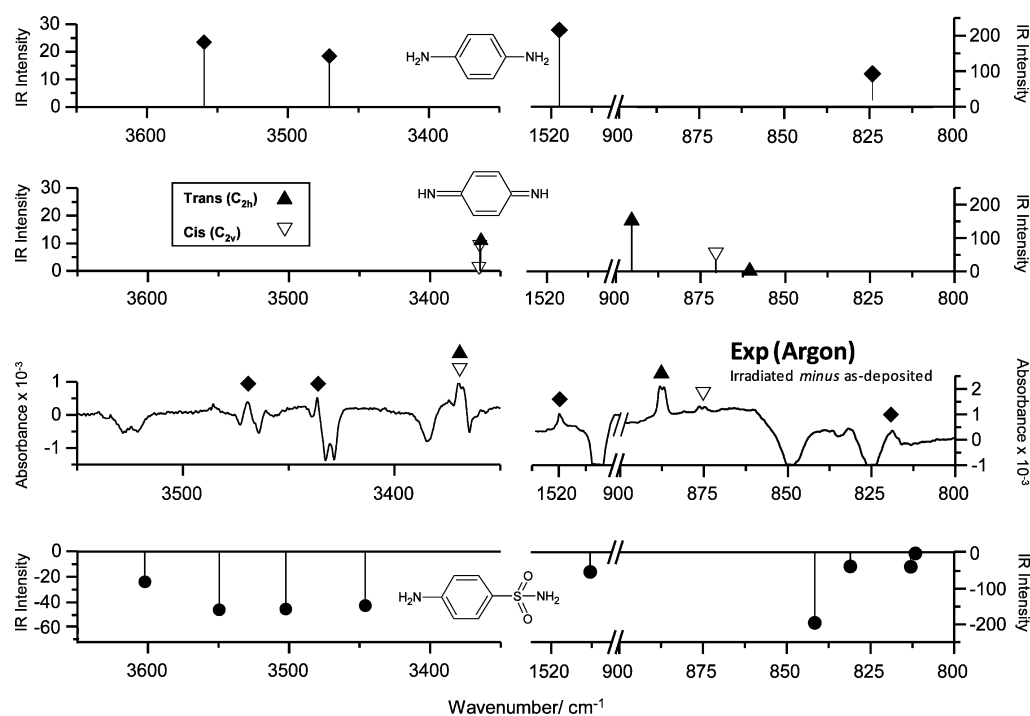


Figure 5. Results of UV ($\lambda > 215$ nm) irradiation of matrix isolated SA (argon matrix data; xenon matrix data are identical): selected spectral ranges testing the production of benzene-1,4-diamine (BDA) and 2,5-cyclohexadiene-1,4-diimine (CHD). Bottom to top: B3LYP/6-311++G(3pd,3df) calculated IR spectrum of SA (spectrum was multiplied by -1), experimental difference spectrum (irradiated matrix minus as-deposited matrix; bands pointing down belong to SA, while those pointing up belong to photoproducts), calculated spectra of CHD (two isomeric forms), and calculated spectrum of BDA. The shift of the wavenumber scale of the experimental spectrum relative to the calculated was done to allow a better comparison between the two sets of data.

case of aniline, the involvement of the aniliny radical in the phototransformation of the compound into CDI is also supported by the observation of several small intensity bands in the spectra of the photolyzed matrices that match well the most intense calculated bands for the radical (see Figure S4 and Table S7).

Neat Solid State Infrared Spectra of SA. As mentioned in the Introduction, the crystal structures of four polymorphs of SA (α , β , γ , and δ) have been determined previously^{15,17–19} (see Figure S1). According to the X-ray diffraction experiments, the NH \cdots O bonds formed by the sulfamide moieties of neighbor molecules in the crystals of all four polymorphs of SA enable a

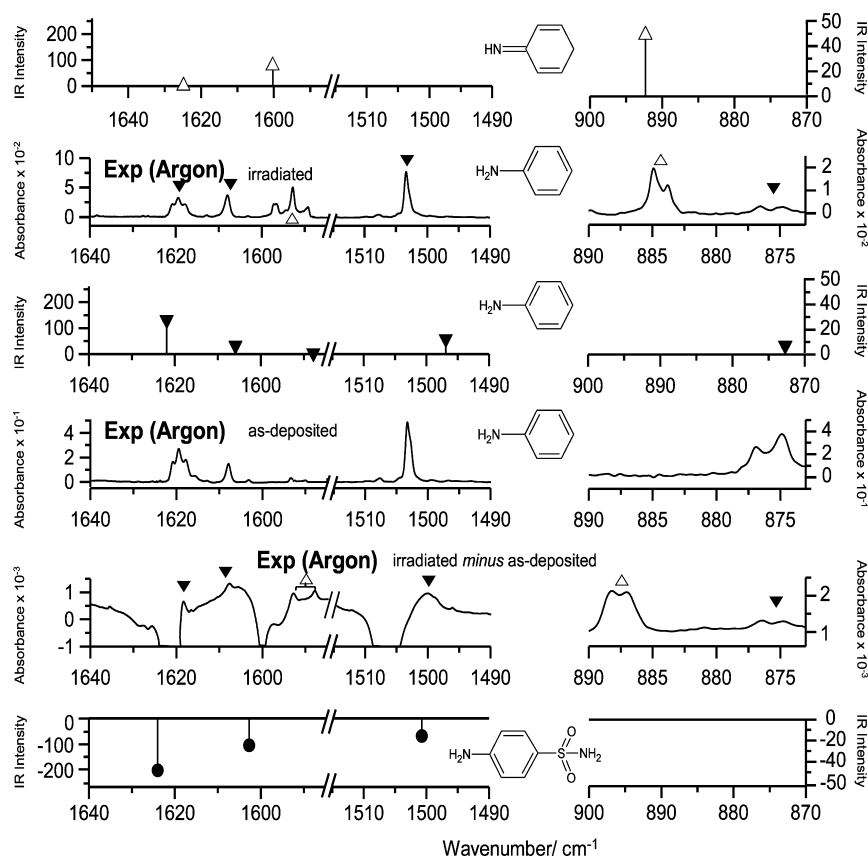


Figure 6. Results of UV ($\lambda > 215$ nm) irradiation of matrix isolated SA (argon matrix data; xenon matrix data are identical): selected spectral ranges testifying the production of aniline and cyclohexa-2,5-dien-1-imine (CDI). Bottom to top: B3LYP/6-311++G(3pd,3df) calculated IR spectrum of SA (spectrum was multiplied by -1), experimental difference spectrum (irradiated matrix minus as-deposited matrix; bands pointing down belong to SA, while those pointing up belong to photoproducts), experimental spectrum of aniline isolated in argon matrix in a dedicated experiment, calculated spectrum of aniline, experimental spectrum of aniline isolated in argon matrix after UV-irradiation ($\lambda > 215$ nm), and calculated spectrum for CDI. The shift of the wavenumber scale of the experimental spectra relative to the calculated was done to allow a better comparison between the two sets of data.

head-to-head contact between adjacent sulfonyl groups, which always result in planes of $\text{NH}\cdots\text{O}$ bonded chains separated by antiparallel stacked aniline fragments. The same dimer unit is present in forms α , γ , and δ polymorphs, which adopt a common topology in the case of α and γ , where one of the two sulfonyl oxygen atoms of each monomeric unit is engaged in an intradimer $\text{NH}\cdots\text{O}$ bond and the second oxygen atom participates in an interdimer $\text{NH}\cdots\text{O}$ bond, in contrast to polymorph δ where just one oxygen atom is employed twice (forming an intra- and an interdimer $\text{NH}\cdots\text{O}$ bond) and the second oxygen atom is free to participate in secondary H-bond interactions with the aniline NH_2 fragment (see Figure S1). In polymorph β , the most interesting feature is the fact that one of the hydrogen atoms of the anilinic NH_2 group is not involved in the H-bond network of the crystal,¹⁶ which, as shown below, has relevant spectroscopic implications. In all cases, the SA molecule adopts the geometry of the lowest-energy conformer I.

In view of the relevance of the dimeric units in the crystalline phases, a series of SA dimers (based on monomeric form I) were investigated theoretically in the present study. The most stable structures are shown in Figure 7. Not surprisingly, the crystallographically relevant centrosymmetric dimer bearing two $\text{NH}\cdots\text{O}$ hydrogen bonds (dimer 1) was found to be the lowest-energy SA dimer. This type of dimer was also found to be the most stable species in other related compounds (e.g., picolinamide,⁶¹ isoniazid,⁶² and pyrazinamide²²). The calculated infrared spectrum for dimer 1 (Figure 8a) was then used to help the assignment of

the experimental spectra obtained for the neat solid compound (Figure 8b–d).

Figure 8b displays the IR spectrum of the purchased commercial sample of SA in a KBr pellet at room temperature. The spectrum corresponds to that of the β -polymorph.^{23,24} A sample of this polymorph was then used in our experiments. The film prepared from sublimating this sample and fast deposition of the obtained vapor onto the cryostat substrate kept at 13 K gave rise to the IR spectrum shown as Figure 8d. It is a typical spectrum of an amorphous phase, with broad bands, in particular in the N–H stretching region, which reveals the characteristic disordered H-bonding network present in an amorphous phase. Upon increasing the temperature, the bands became progressively narrower, due to relaxation to a more ordered state. At about 265 K, the spectrum changes considerably, indicating crystallization of the sample. The obtained spectrum (Figure 8c) is the characteristic one of the γ modification of SA.^{23,24} The proposed band assignments for the spectra of both β and γ polymorphs, based on the calculated spectra for dimer 1, are given in Table 4.

Except in the $\nu\text{N-H}$ stretching region ($3500\text{--}3200\text{ cm}^{-1}$), where the effects of the packing and cooperative H-bonding in the solid states clearly manifest precluding a good reproduction of the experimental spectra by the theoretically predicted spectrum of the SA dimer, the calculated spectrum for the dimer 1 reproduces rather well the experimental data. As it could also be anticipated, in the low frequency range, the failure of the theoretical data obtained for the dimer to reproduce the experimental spectra occurs only

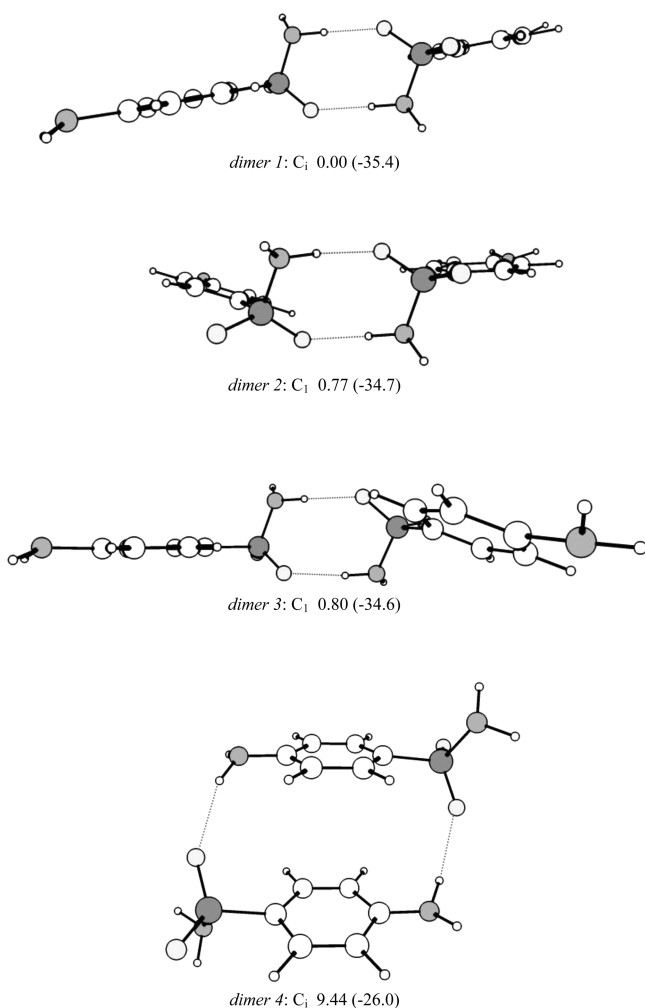
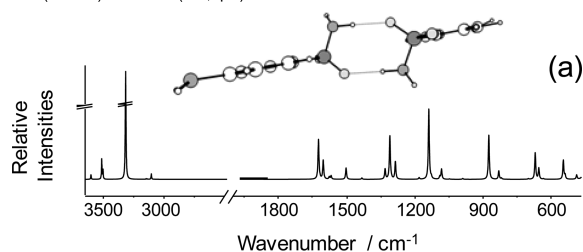


Figure 7. DFT(B3LYP)/6-311++G(3df,3pd) calculated structures for the most stable dimers of SA based on conformer I. Relative energies of the dimers and dimerization energies [calculated as $E(\text{dimer}) - 2 \times E(\text{monomer})$; in parentheses] are given in kJ mol^{-1} . Symmetry point group for each structure is also given.

significantly in the case of the wagging vibrations of the NH_2 groups, which are also known to be extremely sensitive to H-bonding and packing, considerably blue-shifting upon hydrogen bond formation.^{56,63,64} For both wagging modes, the predicted frequencies were too low, particularly in the case of the anilinic NH_2 vibration, because this group is involved in H-bonds in the neat solid phases, whereas it is free in the used dimer 1 model. Nevertheless, the experimental bands associated with these two vibrations are easily recognizable in the spectra due to their expected broadness. Then, the sulfamide NH_2 wagging mode, predicted for the dimer 1 model at 450 cm^{-1} is observed in the spectra of all the solids at about 540 cm^{-1} , while the equivalent vibration of the anilinic NH_2 group is predicted at 671 cm^{-1} and observed as a very broad band spreading the $800\text{--}680 \text{ cm}^{-1}$ spectral region in the glass and γ crystal. On the other hand, in the β polymorph, since one of the hydrogen atoms of the anilinic NH_2 group is not involved in the H-bond network of the crystal,¹⁶ the wagging mode are better described as two independent N–H bending modes and give rise to two bands at 767 and 616 cm^{-1} , the last one ascribable to the non-hydrogen-bonded N–H moiety. Note that the frequency of this last vibration is lower than the predicted one for the dimer 1 model, which points to a considerable weakening of the non-hydrogen-bonded N–H

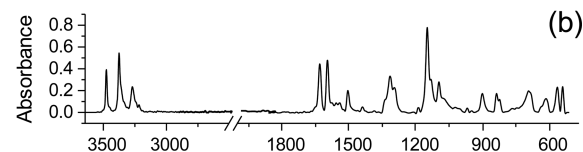
Dimer 1

DFT(B3LYP)/6-311++G(3df,3pd)



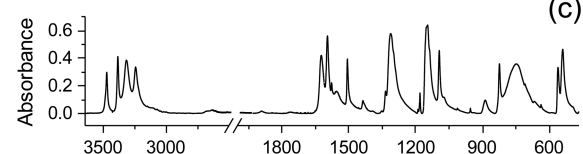
β -Crystal

(room temperature; KBr pellet)



γ -Crystal

($T=265 \text{ K}$; annealed film)



Glass

($T=13 \text{ K}$; film)

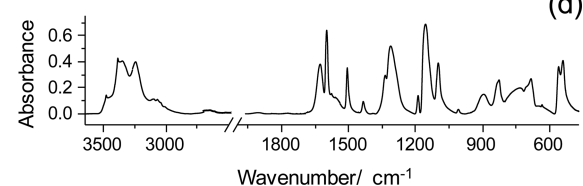


Figure 8. (a) DFT(B3LYP)/6-311++G(3df,3pd) calculated spectrum for SA dimer 1. The calculated wavenumbers were scaled down by a single factor (0.978). (b–d) Infrared spectra of neat condensed phases of SA: glassy state resulting from the fast deposition of the vapor of the compound onto the cryostat's cold substrate at 13 K (d), γ -crystalline state resulting from annealing of the glassy film to 265 K (c), and room temperature β -crystalline phase of the compound in a KBr pellet (b).

bond in the β -crystal. This is indeed in consonance with the X-ray and neutron diffraction results,¹⁶ which indicate that this bond is unusually long. In addition, this singular structural characteristic in the β -crystal does also reflect to some extent in the $\nu\text{N-H}$ stretching region, which for this crystalline variety is considerably distinct of those of the γ -crystal and amorphous state (and also from those of α and δ polymorphs^{23,24}) with only three prominent bands instead of four (see Figure 8).

An interesting point is the fact that crystallization from the low-temperature amorphous state led to the γ -SA polymorph, which is indeed the one corresponding to the stable polymorph at the highest temperatures, before melting.^{23,24} At 265 K , the most stable polymorph is the β -form.²⁴ This behavior contrasts with our previous results on pyrazinamide,²² where the most stable polymorph at the temperature at which the crystallization from the glassy state occurred ($\sim 260 \text{ K}$) was obtained.

A possible explanation for the different behavior in pyrazinamide and SA takes into account the most complex H-bonding networks in the latter molecule, due to the presence of two NH_2 groups and the SO_2 fragment, in contrast to pyrazinamide where

Table 4. Observed Frequencies for Neat SA in the Glassy State Resulting from Fast Deposition of the Vapor of the Compound onto the Cryostat's Cold Substrate at 13 K, in the γ -Crystalline Polymorph Resulting from Annealing of the Glassy Film ($T = 265$ K), and for the Room Temperature β -Polymorph (in KBr Pellet)^a

approximate description	calcd for dimer 1		glass (film, 13 K)	γ -crystal (film, 265 K)	β -crystal (KBr pellet, room temperature)
	frequency	IR intensity			
$\nu(\text{NH}_2)_{\text{as}} 2$	3602.2	46.6	3477	3477	3476
$\nu(\text{NH}_2)_{\text{as}} 1$	3512.5	208.4	3384	3384	3375
$\nu(\text{NH}_2)_{\text{s}} 2$	3502.1	95.4	3349	3315	3357
$\nu(\text{NH}_2)_{\text{s}} 1$	3313.6	826.4	3246	3241	3268
$\nu(\text{C-H})$	3142.8	6.5	3109	3109	3109
$\nu(\text{C-H})$	3132.3	3.0	3049	3109	3089
$\nu(\text{C-H})$	3100.4	32.0	3070	3073	3065
$\nu(\text{C-H})$	3099.9	23.2	3046	3042	3051
$\delta(\text{NH}_2) 1$	1623.3	403.8	1628	1626	1629
ν ring	1602.8	190.6	1599	1597	1595
ν ring	1575.9	24.2	1576	1577	1574
$\delta(\text{NH}_2) 2$	1567.8	35.2	1556	1552	1556/1541
ν ring	1501.6	115.5	1506	1505	1503
ν ring	1432.6	13.7	1436	1437	1437
$\delta(\text{C-H})$	1331.2	103.4	1338	1334	1340
$\nu(\text{S=O})_{\text{as}}$	1310.4	439.4	1313	1311	1315
ν ring	1304.0	9.5	1296	1297	1295
ν ring	1286.3	177.9	1285	1289	1295
$\delta(\text{C-H})$	1182.6	16.0	1187	1191/1182	1188
$\nu(\text{S=O})_{\text{s}}$	1139.9	707.7	1153	1154/1147	1148
$\delta(\text{C-H})$	1128.7	19.2	1134	1137	1132
$\gamma(\text{NH}_2) 1$	1091.2	28.5	1097	1093	1096
δ ring	1083.4	102.2	1097	1093	1096
$\gamma(\text{NH}_2) 2$	1048.2	3.7	n.o.	1072	1071
$\gamma(\text{C-H})$	989.3	8.8	1009	1012	1021/1001
$\gamma(\text{C-H})$	967.0	0.6	955	955	969
$\gamma(\text{C-H})$	948.9	0.1	944	940	949
$\nu(\text{S-N})$	873.8	446.5	899	890	901
$\gamma(\text{C-H})$	830.0	84.3	836	826	838
$\gamma(\text{C-H})$	818.6	12.5	828	n.o.	824
δ ring	811.5	0.6	n.o.	n.o.	n.o.
τ ring	700.6	6.2	702	709	694
$w(\text{NH}_2) 1$	670.8	274.4	799–677	802–677	767/616 ^b
$\delta(\text{N-SO}_2)_{\text{s}}$	655.0	114.6	684	666	685
δ ring	635.1	5.9	634	637	639
$\delta(\text{N-SO}_2)_{\text{as}}$	548.0	196.0	560	561	565
$\gamma(\text{C-N})$	540.3	41.5	560	561	565
δ ring	489.9	43.5	500	495	n.i.
$\gamma(\text{N-SO}_2)$	463.6	79.0	458	458	n.i.
$w(\text{NH}_2) 2$	450.5	675.1	540	540	541

^aThe DFT(B3LYP)/6-311++G(3df,3pd) calculated spectrum for dimer 1, used to help the assignment of the experimental spectra, is also provided. Calculated frequencies (scaled by 0.978) in cm^{-1} , calculated intensities in km mol^{-1} . ν , bond stretching; δ , bending; γ , rocking; τ , torsion; w , wagging; s , symmetric; as , antisymmetric; n.o., not observed; n.i., not investigated. See Table S2 for definition of coordinates. ^bFor this crystal, the NH_2 wagging vibration is better described as two independent N–H bending modes (see text).

only one NH_2 group is present together with the ring N atom H-bond acceptor. Such increased complexity of the H-bond network in SA may comparatively difficult the conversion of the kinetically preferred γ -polymorph (which has in average longer H-bonds than the β -form;^{15–18,22} note that, in consonance with this, the IR spectrum of the γ -polymorph also resembles more that of the amorphous solid, see Figure 8) into the thermodynamically preferred β -polymorph. Nevertheless, it must be recalled that the microscopic mechanisms of crystal formation are far from being well understood, so that an extensive systematic work is still required to duly explore the possibility of using cold crystallization from a low temperature amorphous state, to

produce specific crystalline phases. Recent studies^{65–68} consider that polymorphism might already be a property of the metastable glassy (or supercooled liquid) state, pointing to the greater relevance of precursor locally bond-oriented regions to the nucleation processes compared to locally denser regions, and considering that those precursor regions not only act as seeds of the nucleation process, but may also determine the particular polymorph which is to be nucleated from them.

CONCLUSION

In this work, the conformational preferences and spectroscopic properties of SA have been studied by FTIR spectroscopy for the

compound: (a) isolated in cryogenic matrices (argon and xenon) and (b) in neat condensed phases. The experimental studies were partially grounded on density functional theory calculations performed at the B3LYP/6-311++G(d,p) and B3LYP/6-311++G(3df,3pd) levels of theory.

The full conformational search on the potential energy surface allowed the identification of four experimentally relevant low-energy conformers, all of them with relative energies below 2 kJ mol⁻¹, and expected to be populated in the gas phase. The relative stability of the conformers was explained based on different intramolecular interactions (bond–dipole interactions; NH··· π H-bond type interactions). Barriers for conformational isomerization were also calculated. The low values obtained for most of these barriers (associated either with internal rotations or inversion at the nitrogen atoms) led to the expectation that only the most stable conformer (I) would survive to the process of deposition of the cryogenic matrices and would then be the sole species present in both the argon and xenon matrices. Such expectation was indeed confirmed experimentally.

Upon broadband UV irradiation ($\lambda > 215$ nm), two photofragmentation pathways were observed, the dominant process leading to extrusion of sulfur dioxide and simultaneous formation of benzene-1,4-diamine, which is also converted into 2,5-cyclohexadiene-1,4-diimine along the irradiation experiments. A second, minor photoprocess was also observed, consisting in the γ -cleavage plus^{1,3} H-atom migration from the sulfamide group to the aromatic ring. This reaction leads to formation of iminosulfane dioxide and aniline. Aniline can then undergo a subsequent photoconversion into cyclohexa-2,5-dien-1-imine, in a process which was found to be similar to the transformation of phenol into 2,5-cyclohexadienone.⁶⁰ Observation of 4-aminoanilino and aniliny radicals indicates that the observed photoprocesses were radical in nature, also, in a similar way to what was found previously for phenol.⁶⁰

Finally, the crystalline polymorph of SA resulting from warming (265 K) the amorphous solid obtained from fast cooling of the vapor of the compound onto the cold (13 K) substrate of the cryostat was identified spectroscopically, and found to be the γ crystalline phase, the one exhibiting in average longer H-bonds and an infrared spectrum resembling more that of the low temperature SA glass. Full assignment of the infrared spectra of this crystalline variety as well as of those of the β -polymorph room temperature crystalline sample and low temperature amorphous state was undertaken with help of theoretical results obtained for the crystallographically relevant dimer of SA, which was also shown to correspond to the most stable dimer of sulfanilamide.

■ ASSOCIATED CONTENT

■ Supporting Information

Figure S1 with a schematic representation of the main constituting units of the four polymorphs of SA. Figure S2 with the torsional interconversion potential energy profiles between SA conformers. Figure S3 with the calculated IR spectra of the four conformers of SA. Figure S4 with the infrared spectra of as-deposited SA matrix (in argon), same matrix after irradiation ($\lambda < 215$ nm), and difference spectrum (irradiated minus as-deposited) in the 675–500 (top) and 1120–1095 (bottom) cm⁻¹ spectral regions. Figure S5, with kinetic data for photochemical experiments. Table S1 with the DFT(B3LYP)/6-311++G(d,p) and 6-311++G(3df,3pd) optimized geometries for the four conformers of SA. Tables S2–S6, with the definition of the symmetry coordinates and results of normal coordinates

analysis for the four conformers of SA. Table S7, with the experimentally observed and calculated frequencies, and calculated infrared intensities for the 4-aminoanilino and aniliny radicals. Table S8, with the full calculated infrared spectra for all observed photoproducts resulting from irradiation of matrix-isolated SA. This material is available free of charge via the Internet at <http://pubs.acs.org>.

■ AUTHOR INFORMATION

Corresponding Author

*E-mail: rfausto@ci.uc.pt.

Notes

The authors declare no competing financial interest.

■ ACKNOWLEDGMENTS

This work was supported by Fundação para a Ciência e a Tecnologia (FCT, Project PTDC/QUI-QUI/111879/2009, also supported by QREN-COMPETE and the European Union), ANPCyT (PICT(2011)/0226), CONICET (PIP 114-201101-00024), CYTED (312RT0463). A.B. acknowledges FCT for the award of a Post-Doctoral Grant (SFRH/BPD/66154/2009). A.G.Z. is member of the Research Career of CONICET (National Research Council, Argentina).

■ REFERENCES

- (1) Gelmo, P. J. *Prakt. Chem. (Leipzig)* **1908**, 77, 369.
- (2) Domagk, G. *Dtsch. Med. Wschr.* **1940**, 66, 203.
- (3) Domagk, G. *Chirurg.* **1941**, 13, 433.
- (4) Grundmann, E. Gerhardt Domagk: The First Man to Triumph over Infectious Diseases; LIT Verlag Münster: Berlin, 2004.
- (5) Blasco, F.; Perelló, L.; Latorre, J.; Borrás, J.; García-Granda, S. J. *Inorg. Biochem.* **1996**, 61, 143.
- (6) Supuran, C. T.; Mincione, F.; Scozzafava, A.; Briganti, F.; Mincione, G.; Ilies, M. A. *Eur. J. Med. Chem.* **1998**, 33, 247.
- (7) Ferrer, S.; Borrás, J.; Garciaespana, E. *J. Inorg. Biochem.* **1990**, 39, 297.
- (8) Joshi, S.; Khosla, N.; Khare, D.; Tiwari, P. *Acta Pharm.* **2002**, 52, 197.
- (9) Zondhi, S. M.; Johar, M.; Singhal, N.; Dastidar, S. G.; Shukla, R.; Raghbir, R. *Mon. Chem.* **2000**, 131, 511.
- (10) Supuran, C. T.; Scozzafava, A.; Casini, A. *Med. Res. Rev.* **2003**, 23, 146.
- (11) Li, J. J.; Anderson, G. D.; Burton, E. G.; Cogburn, J. N.; Collins, J. T.; Garland, D. J.; Gregory, S. A.; Huang, H. C.; Isakson, P. C.; Koboldt, C. M.; Logusch, E. W.; Norton, M. B.; Perkins, W. E.; Reinhard, E. J.; Seibert, K.; Veenhuizen, A. W.; Zhang, Y.; Reitz, D. B. *J. Med. Chem.* **1995**, 38, 4570.
- (12) Byrn, S. R.; Pfeiffer, R. R.; Stowell, J. G. *Solid-State Chemistry of Drugs*; Academic Press: Waltham, MA, 1982.
- (13) Watanabe, A. *Naturwiss* **1941**, 29, 116.
- (14) Yakowitz, M. L. *J. Assoc. Official Agric. Chem.* **1948**, 31, 656.
- (15) Alleaume, M.; Decap, V. *Acta Crystallogr.* **1965**, 18, 731.
- (16) O'Connell, A. M.; Maslen, E. N. *Acta Crystallogr.* **1967**, 22, 134.
- (17) O'Connor, B. H.; Maslen, E. N. *Acta Crystallogr.* **1965**, 18, 363.
- (18) Alleaume, M.; Decap, J. *Acta Crystallogr.* **1965**, 19, 934.
- (19) Gelbrich, T.; Bingham, A. L.; Threlfall, T. L.; Hursthouse, M. B. *Acta Crystallogr., Sect. C: Cryst. Struct. Commun.* **2008**, 64, O205.
- (20) Toscani, S.; Dzyabchenko, A.; Agafonov, V.; Dugue, J.; Ceolin, R. *Pharm. Res.* **1996**, 13, 151.
- (21) Toscani, S. *Thermochim. Acta* **1998**, 321, 73.
- (22) Borba, A.; Albrecht, M.; Gómez-Zavaglia, A.; Suhm, M. A.; Fausto, R. *J. Phys. Chem. A* **2010**, 114, 151.
- (23) Lin, H. O.; Guillory, J. K. *J. Pharm. Sci.* **1970**, 59, 972.
- (24) Sekiguchi, K.; Tsuda, Y.; Kanke, M. *Chem. Pharm. Bull.* **1975**, 23, 1353.

- (25) Baxter, J. N.; Cymermancraig, J.; Willis, J. B. *J. Chem. Soc.* **1955**, 669.
- (26) Topaçli, A.; Kesimli, B. *Spectrosc. Lett.* **2001**, *34*, 513.
- (27) Topaçli, C.; Topaçli, A. *Spectrosc. Lett.* **2002**, *35*, 207.
- (28) Topaçli, C.; Topaçli, A. *J. Mol. Struct.* **2003**, *644*, 145.
- (29) Varghese, H. T.; Panicker, C. Y.; Anto, P. L.; Philip, D. *J. Raman Spectrosc.* **2006**, *37*, 487.
- (30) Varghese, H. T.; Panicker, C. Y.; Philip, D. *Spectrochim. Acta A* **2006**, *65*, 155.
- (31) López-Sánchez, M.; Ruedas-Rama, M. J.; Ruiz-Medina, A.; Molina-Díaz, A.; Ayora-Canada, M. J. *Talanta* **2008**, *74*, 1603.
- (32) Halim, M. A.; Shaw, D. M.; Poirier, R. A. *THEOCHEM* **2010**, *960*, 63.
- (33) Soriano-Correa, C.; Esquível, R. O.; Sagar, R. P. *Int. J. Quantum Chem.* **2003**, *94*, 165.
- (34) Gomes, J. R. B.; Gomes, P. *Tetrahedron* **2005**, *61*, 2705.
- (35) Popova, A. D.; Georgieva, M. K.; Petrov, O. I.; Petrova, K. V.; Velcheva, E. A. *Int. J. Quantum Chem.* **2007**, *107*, 1752.
- (36) Ildiz, G. O.; Akyuz, S. *Vibrat. Spectrosc.* **2012**, *58*, 12.
- (37) Motten, A. G.; Chignell, C. F. *Photochem. Photobiol.* **1983**, *37*, 17.
- (38) Liu, Z. T.; Zhang, H. Y.; Shao, B.; Zhao, R. *Nucl. Instrum. Methods Phys. Res., Sect. B* **2006**, *252*, 285.
- (39) Weiss, B.; Durr, H.; Haas, H. *J. Angew. Chem.* **1980**, *19*, 647.
- (40) Boreen, A. L.; Arnold, W. A.; McNeill, K. *Abstr. Pap. Am. Chem. Soc.* **2004**, *228*, 287.
- (41) Borba, A.; Gómez-Zavaglia, A.; Simões, P. N. N. L.; Fausto, R. *J. Phys. Chem. A* **2005**, *109*, 3578.
- (42) Almeida, R.; Gómez-Zavaglia, A.; Kaczor, A.; Ismael, A.; Cristiano, M. L. S.; Fausto, R. *J. Mol. Struct.* **2009**, *938*, 198.
- (43) Frisch, M. J.; Trucks, G. W.; Schlegel, H. B.; Scuseria, G. E.; Robb, M. A.; Cheeseman, J. R.; Montgomery, J., J. A.; Vreven, T.; Kudin, K. N.; Burant, J. C.; Millam, J. M.; Iyengar, S. S.; Tomasi, J.; Barone, V.; Mennucci, B.; Cossi, M.; Scalmani, G.; Rega, N.; Petersson, G. A.; Nakatsuji, H.; Hada, M.; Ehara, M.; Toyota, K.; Fukuda, R.; Hasegawa, J.; Ishida, M.; Nakajima, T.; Honda, Y.; Kitao, O.; Nakai, H.; Klene, M.; Li, X.; Knox, J. E.; Hratchian, H. P.; Cross, J. B.; Bakken, V.; Adamo, C.; Jaramillo, J.; Gomperts, R.; Stratmann, R. E.; Yazyev, O.; Austin, A. J.; Cammi, R.; Pomelli, C.; Ochterski, J. W.; Ayala, P. Y.; Morokuma, K.; Voth, G. A.; Salvador, P.; Dannenberg, J. J.; Zakrzewski, V. G.; Dapprich, S.; Daniels, A. D.; Strain, M. C.; Farkas, O.; Malick, D. K.; Rabuck, A. D.; Raghavachari, K.; Foresman, J. B.; Ortiz, J. V.; Cui, Q.; Baboul, A. G.; Clifford, S.; Cioslowski, J.; Stefanov, B. B.; Liu, G.; Liashenko, A.; Piskorz, P.; Komaromi, I.; Martin, R. L.; Fox, D. J.; Keith, T.; Al-Laham, M. A.; Peng, C. Y.; Nanayakkara, A.; Challacombe, M.; Gill, P. M. W.; Johnson, B.; Chen, W.; Wong, M. W.; Gonzalez, C.; Pople, J. A. *Gaussian 03*, Revision B. 01; Gaussian, Inc., Wallingford, CT, 2004.
- (44) Becke, A. D. *Phys. Rev. A* **1988**, *38*, 3098.
- (45) Lee, C. T.; Yang, W. T.; Parr, R. G. *Phys. Rev. B* **1988**, *37*, 785.
- (46) Vosko, S. H.; Wilk, L.; Nusair, M. *Can. J. Phys.* **1980**, *58*, 1200.
- (47) McLean, A. D.; Chandler, G. S. *J. Chem. Phys.* **1980**, *72*, 5639.
- (48) Krishnan, R.; Binkley, J. S.; Seeger, R.; Pople, J. A. *J. Chem. Phys.* **1980**, *72*, 650.
- (49) Frisch, M. J.; Pople, J. A.; Binkley, J. S. *J. Chem. Phys.* **1984**, *80*, 3265.
- (50) Ditchfield, R.; Miller, D. P.; Pople, J. A. *J. Chem. Phys.* **1971**, *54*, 4186.
- (51) Csaszar, P.; Pulay, P. *J. Mol. Struct.* **1984**, *114*, 31.
- (52) Gómez-Zavaglia, A.; Ismael, A.; Cabral, L. I. L.; Kaczor, A.; Paixão, J. A.; Fausto, R.; Cristiano, M. L. S. *J. Mol. Struct.* **2011**, *1003*, 103.
- (53) Schachtschneider, J. H.; Mortimer, F. S. *Vibrational Analysis of Polyatomic Molecules. VI. FORTRAN IV Programs for Solving the Vibrational Secular Equation and for the Least-Squares Refinement of Force Constants*, Project No. 31450. *Structural Interpretation of Spectra*; Shell Development Co: Houston, TX, 1965.
- (54) Peng, C.; Schlegel, H. *Isr. J. Chem.* **1994**, *33*, 449.
- (55) Reva, I. D.; Stepanian, S. G.; Adamowicz, L.; Fausto, R. *Chem. Phys. Lett.* **2003**, *374*, 631.
- (56) Borba, A.; Gómez-Zavaglia, A.; Fausto, R. *J. Mol. Struct.* **2006**, *794*, 196.
- (57) Gómez-Zavaglia, A.; Reva, I. D.; Frija, L.; Cristiano, M. L.; Fausto, R. *J. Phys. Chem. A* **2005**, *109*, 7967.
- (58) Barnes, A. J. *J. Mol. Struct.* **1984**, *113*, 161.
- (59) Svensson, T.; Nelander, B. *Chem. Phys.* **2003**, *286*, 347.
- (60) Akai, N.; Kudoh, S.; Nakata, M. *J. Phys. Chem. A* **2003**, *107*, 6725.
- (61) Giuliano, B. M.; Reva, I.; Lapinski, L.; Fausto, R. *J. Chem. Phys.* **2012**, *135*, 02450.
- (62) Borba, A.; Albrecht, M.; Gomez-Zavaglia, A.; Lapinski, L.; Nowak, M. J.; Suhm, M. A.; Fausto, R. *Phys. Chem. Chem. Phys.* **2008**, *10*, 7010.
- (63) Borba, A.; Gomez-Zavaglia, A.; Fausto, R. *J. Phys. Chem. A* **2009**, *113*, 9220.
- (64) Rozenberg, M.; Shoham, G.; Reva, I. D.; Fausto, R. *Spectrochim. Acta, Part A* **2004**, *60*, 2319.
- (65) Rozenberg, M.; Shoham, G.; Reva, I. D.; Fausto, R. *Spectrochim. Acta, Part A* **2004**, *60*, 463.
- (66) Russo, J.; Tanaka, H. *Sci. Rep.* **2012**, *2*, art. 505.
- (67) Tanaka, H.; Kawasaki, T.; Shintani, H.; Watanabe, K. *Nat. Mater.* **2010**, *9*, 324.
- (68) Tanaka, H. *J. Stat. Mech.: Theory Exp.* **2010**, *2010*, 12001.